TÜBİTAK

Turkish Journal of Chemistry

http://journals.tubitak.gov.tr/chem/

Research Article

Turk J Chem
(2018) 42: 221 – 236

doi:10.3906/kim-1605-35

Experimental and theoretical studies of carbazole-based Schiff base as a fluorescent Fe^{3+} probe

Hakan KANDEMİR[1], Abdulkadir KOÇAK[2], Süreyya Oguz TÜMAY[2], Bünyemin ÇOŞUT[2], Yunus ZORLU[2], İbrahim Fazil ŞENGÜL[2,*]

[1]Department of Chemistry, Faculty of Arts and Science, Namık Kemal University, Tekirdağ, Turkey
[2]Department of Chemistry, Faculty of Science, Gebze Technical University, Gebze, Kocaeli, Turkey

Received: 17.05.2016 • **Accepted/Published Online:** 10.09.2016 • **Final Version:** 27.04.2018

Abstract: Synthesis of a new (E)-N1-((9-ethyl-9H-carbazol-3-yl)methylene)-5-nitrobenzene-1,2-diamine as a fluorescent chemosensor for selective detection of Fe^{3+} ion over a number of other metal ions is described. The method for the synthesis of the carbazole Schiff base was based on the condensation of carbazole-3-carbaldehyde with 4-nitro-o-phenyldiamine in dimethylformamide in a moderate yield. The structure of the final compound was characterized by ^{1}H NMR, ^{13}C NMR, IR, mass spectrometry, and single crystal X-ray diffraction. The final compound exhibited exceptional selective and sensitive turn-on fluorescence response to the Fe^{3+} cation. The fluorescent intensity of the final compound was increased 20-fold and the stoichiometry ratio of the final compound to Fe^{3+} was 1:1. The association constant and detection limit for Fe^{3+} ion were predicted from fluorescence titrations as $(1.36 \pm 0.09).10^{4}$ M^{-1} and 1.0 to 6.0 μM, respectively. The photophysical behavior of the compound was further explored by DFT methods. The predicted UV-Vis spectrum by TDDFT calculations was compared to the observed absorption spectrum of the targeted compound.

Key words: Schiff base, carbazole, Fe^{3+} ion, sensor, fluorescence enhancement, TD-DFT calculations

1. Introduction

The design and synthesis of fluorescent chemosensors has been the subject of intense study because of their potential application in supramolecular chemistry, organic chemistry, drug delivery, biological chemistry, and environmental research.[1−3] They have been desired to have important sensitivity and selectivity for detecting metal ions in both aqueous and nonaqueous media.[4−7] For that purpose, many chemosensors have been developed, in particular, for transition metals such as Ca, Hg, Cu, and Zn.[8−13] Among all the transition metals, Fe is the most abundant in the human body.[14] It is an essential element for normal physiological function in the human body because of its involvement in many critical cellular processes such as energy productivity, oxygen transport, DNA synthesis, and regulation of gene expression.[15−17] Additionally, iron is a key co-factor of many cellular enzymes such as oxidases, catalases, cytochromes, nitric oxide synthases, and ribonucleotide reductases.[17] Either iron overload or iron deficiency can cause cellular damage and diseases such as liver damage, anemia, diabetes, hemochromatosis, Parkinson disease, and cancer.[18−20] Consequently, much attention has been devoted to the development of highly selective fluorescent chemosensors for Fe^{3+} to satisfy biological and environmental applications. To date, there have been some good chemosensors for iron, but with

*Correspondence: fazilsengul@gtu.edu.tr

limited detection limit down to the ppm level. They include selectivity to Fe^{2+} and/or Fe^{3+}.[21–23] However, these sensors have very limited applications in living cells and so developing new candidate chemosensors will help us gain insights into iron cellular biology.[33]

Schiff base derivatives are an important class of compounds due to their broad pharmaceutical effects including antibacterial, antifungal, and antitumor activity.[34,35] The main advantage of C=N moiety is that they bind to metal ions via their nitrogen lone pair to generate metal complex.[36] Since C=N isomerization is the predominant decay process of the excited molecule, Schiff bases with a bridged C=N structure are often known as nonfluorescent.[28,37] However, inhibition of the C=N isomerization gives the opportunity to show strong fluorescence for such molecules.[28,37] Inhibition can be done either by attaching bridge atoms between C and N of C=N or by coordinating the N with transition metal ions.[28,37]

Carbazole and its derivatives are also an important class of nitrogen-containing heterocyclic compounds, having long attracted attention from researchers due to their valuable properties.[38] Carbazole-based compounds are attractive as photoelectrical functional materials and dyes and as well as for supramolecular recognition and medicinal chemistry.[38] Another significant feature of carbazole is that its ring is easily functionalized and can be covalently linked to other molecules.[39] As a result of this feature, carbazole is widely used as a building block.[40] The paramagnetic Fe^{3+} is a well-known quencher[28] and so it is difficult to develop a fluorescent chemosensor since it suppresses the fluorescence of the ligand. On the other hand, carbazole derivatives have reportedly been promising candidates for selective detection of Fe^{3+}.[41]

In the current study, we report the preparation of compound **3** bridged C=N structure, which shows outstanding selective recognition to Fe^{3+}, potentially binding through N atoms of the amine and C=N double bond and inhibiting C=N isomerization. The selective recognition of Fe^{3+} ion interacting with compound **3** can be detected by both UV-Vis absorption and fluorescence emission methods in ppm levels. In addition, we performed DFT calculations in order to obtain insights into the photophysical behavior of compound **3** and possible binding mode to the Fe^{3+}.

2. Results and discussion

2.1. Synthesis and characterization

The synthesis of carbazole-linked Schiff base began with the formylation of *N*-ethylcarbazole **1** via the Vilsmeier–Haack method, using $POCl_3$/DMF to obtain carbazole-3-carbaldehyde **2** in 70% yield (Scheme).[42] With the carbazole-3-carbaldehyde **2** in hand, it was of interest to generate carbazole-linked Schiff base **3**. Treatment of carbazole-3-carbaldehyde **2** with 4-nitro-o-phenyldiamine in dimethylformamide at 80 °C gave the corresponding base **3** as crude product, which purified via column chromatography in 46% yield.

To the best of our knowledge, compound **3** is novel and its structure was established with the help of spectroscopic data. The ^{1}H NMR spectrum of **3** showed the replacement of the aldehyde proton at 10.11 ppm by the new imine proton at 8.88 ppm. Moreover, the ^{13}C NMR spectrum demonstrated the imine carbon at 160.6 ppm. The disappearance of the CHO proton for the spectrum of starting materials **2** and the appearance of the CH=N proton indicated that a Schiff base had occurred. The IR spectrum exhibited an imine stretching frequency at 1679 cm^{-1}. Further structural verification was obtained via mass spectroscopy, with MALDI mass spectra revealing an $(M+H)^+$ peak at m/z 359, consistent for compound **3**.

The solid state structure of the compound **3** was further confirmed by X-ray crystallography (Figure 1). Compound **3** crystallizes in the monoclinic space group $P2_1/n$ with two crystallographically different Schiff

base molecules in the asymmetric unit cell. The azomethine double bond (–C–C=N–C–) of both Schiff base molecules has an E-configuration. The bond lengths and internal bond angles of the 13-membered carbazolyl-fused ring system are comparable to those observed in similar compounds.[43,44] The dihedral angle between the plane of the phenyl ring and the plane of the carbazole skeleton is 47.24 (9)° in molecule A and 43.57° in molecule B. Two symmetry independent molecules are linked via hydrogen bonds (H1N···O1 and H4N···O3) to form a one-dimensional hydrogen-bonded infinite chain along the c direction of the unit cell.

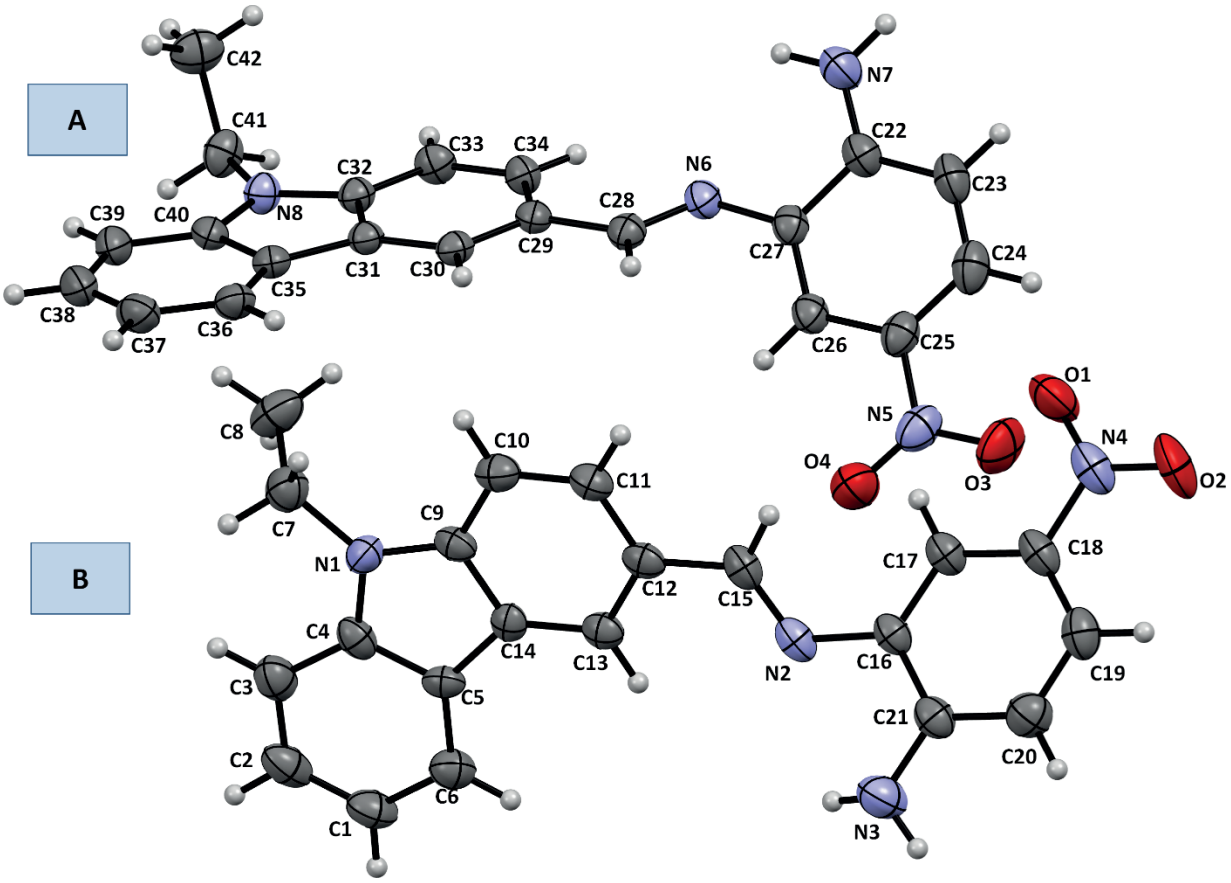

Figure 1. The asymmetric unit of compound 3. Displacement ellipsoids are drawn at the 30% probability level. H-atoms are shown as small spheres of arbitrary radii.

In order to find best conformation of compound **3**, we carried out ground state DFT calculations at B3LYP/6-311++G(d,p) level in the gas phase and PCM description of the ACN environment. Compound **3** has E- and Z-isomers around the C=N bond along with torsions of ethyl-, nitro-, amine-, phenyl-, and carbazole-ring groups. From the calculations, we evaluated that these torsions have small potential barriers on the corresponding coordinates. The torsion on the carbazole ring forms two energetically degenerate conformations, which are also experimentally observed (molecule A and molecule B on the crystal structures: $\Delta\ E(B-A) =$ 0.14 kcal/mol). The angles on the planes of the phenyl ring and carbazole ring also perfectly match the crystal structure (molecule A: 41.3°, and molecule B: 41.2°). We also calculated a possible Z-isomer that was not observed crystallographically. The E-isomer is remarkably more stable than the Z-isomer (by 6.88 kcal/mol). Furthermore, we calculated the transition state (in the gas phase) between E- and Z-isomers in order to see whether the barrier is achievable. The transition state lies 22.78 kcal/mol above the most stable E-isomer.

Since this value is smaller the UV-Vis photon energy, absorption of one photon can easily promote sufficient energy to overcome this barrier. This suggests that photo-excited compound **3** has a potential decay of C=N isomerization.

2.2. Absorption properties

The cation binding properties of compound **3** were investigated by using both UV-vis and fluorescence methods. Figure 2a shows the absorption spectrum of compound **3** (10 μM in acetonitrile). The spectrum consists of a broad band peaking at 380 nm (ε = 29,680 L.mol^{-1}.cm^{-1}) and a relatively narrow band at 292 nm (ε = 32,340 L.mol^{-1}.cm^{-1}). For such systems, it was reported that the low lying band is due to $\pi - \pi^*$ transition, while the higher wavelength bands are due to solvent perturbed intraligand electronic transition.[45–47] Thus, the peak at 292 nm is likely due to $\pi - \pi^*$ transition of the C=N group and the 380 nm band is due to the intraligand charge transfer (ILCT) band of the entire conjugated molecule.[2,48]

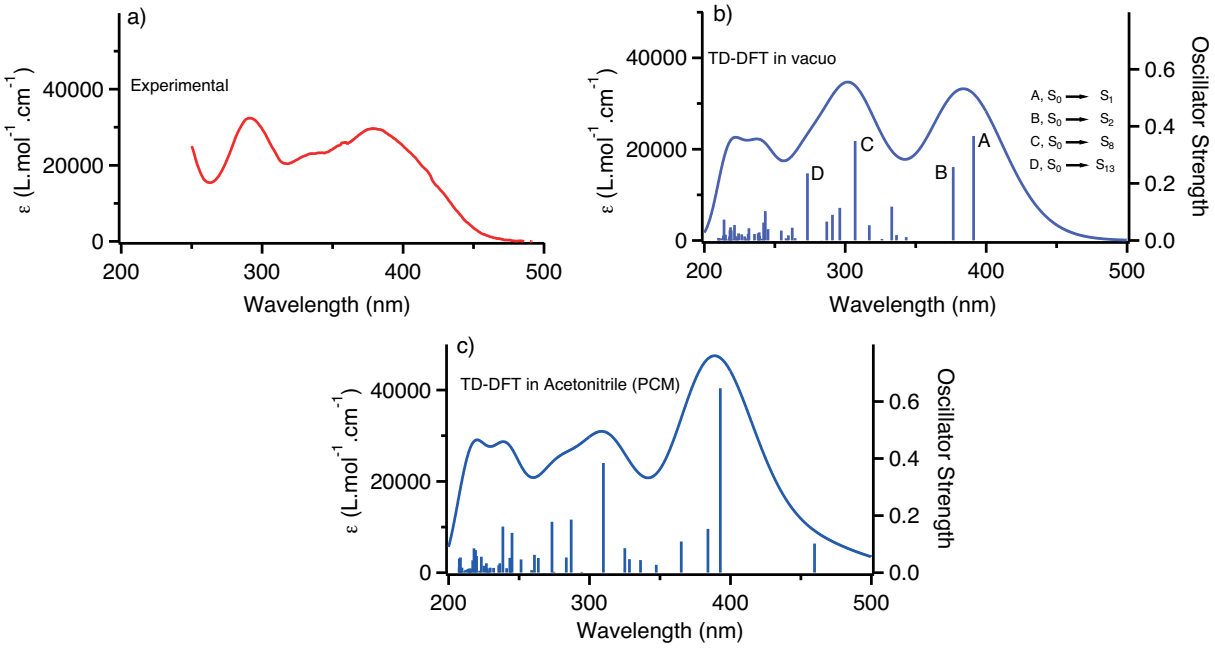

Figure 2. Comparison of a) experimental absorption spectrum (top) with the simulation of TDDFT calculations, b) in vacuo (middle), and c) in PCM description of acetonitrile solvent (bottom) for compound 3. The calculations use B3LYP/6-311++G(d,p). Vertical lines on the calculated spectra represent the oscillator strengths (right axis). The molar extinction coefficients are calculated as discussed in the text. Simulations use Gaussian band shape with 4000 cm^{-1} full-width at half-maximum (fwhm). The labels show the transition occurring to the regarding excited state.

In order to gain insight into the observed spectrum, we carried out TDDFT calculations both in vacuo (Figure 2b) and with PCM description of acetonitrile solvent (Figure 2c). Important vertical excitations and their corresponding transitions are shown in Table 1. The calculations on the gas phase show better fit to the experimental spectrum. In the gas phase, the most intense (allowed) transitions are mostly HOMO$\rightarrow$LUMO (Label A on Figure 2b, surfaces on Figure 3) and HOMO$\rightarrow$LUMO+1 (Label B on Figure 2b) at 382 nm corresponding to the observed 380 nm peak. The other intense band, at 302 nm, corresponding to an experimental value of 292 nm, is a combination of multiple transitions.

Table 1. Experimental and calculated peak positions with transition intensities for compound 3. Calculations are at B3LYP/6-311++G(d,p).

	Dominant transition	Vertical excitation (nm)	Oscillator strength[a]	Abs. peak, λ (nm)	Energy, $\tilde{\nu}$ (cm^{-1})	Coefficient, ε ($L.mol^{-1}.cm^{-1}$)
Experiment				380 292	26,178 34,247	29,680 32,340
TDDFT, *vacuo*	$S_0 \rightarrow S_1$	391.06 (428.84*)	0.3663	382	26,316	33,170
	$S_0 \rightarrow S_2$	376.63	0.2577			
	$S_0 \rightarrow S_8$	307.01	0.3488	302	33,113	34,710
	$S_0 \rightarrow S_{13}$	273.17	0.2353			
TDDFT, acetonitrile	$S_0 \rightarrow S_2$	392.83	0.6464	389	25,707 32,362	47,510 30,960
	$S_0 \rightarrow S_9$	309.83	0.3844	309		

*Adiabatic excitation. [a]: Only oscillator strength values greater than 0.20 are listed.

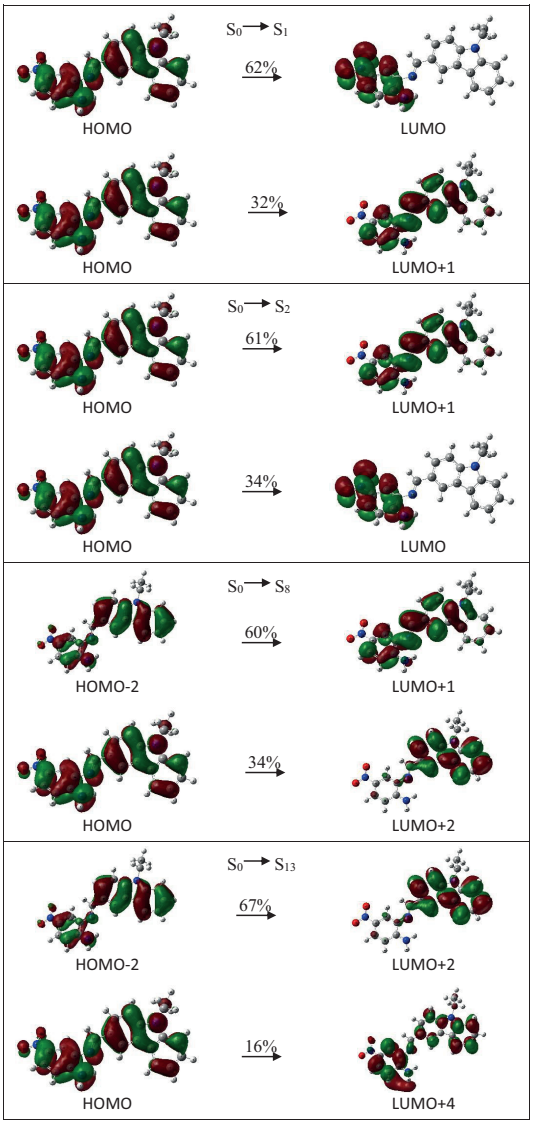

Figure 3. Ground state molecular orbitals' SCF density surfaces (isoval = 0.002) along with expected dominant transitions and contributions of the TDDFT calculation at the ground state geometry. Calculations use B3LYP/6-311++G(d,p).

Figure 3 shows the ground state SCF-type molecular orbitals (MOs) of the valence electrons of compound **3** along with contributions of each orbital from a TDDFT calculation. As can be seen from Figure 3, all transitions include remarkable electron density flow between carbazole ring and phenyl ring, which is indicative of ILCT. The C=N bond plays a bridge role in this π-conjugation and thus electron density flow.

In addition, we also carried out natural transition orbital (NTO) analysis, which is a compact orbital representation for the electronic transition density matrix and gives a maximal correspondence between the orbitals the excitation occurs from (hole) and the excitation occurs to (particle).[49] Highly mixed canonical SCF molecular orbitals of the TDDFT calculations are much better represented by the NTO analysis. It shows that all the UV-Vis bands include both $\pi - \pi^*$ and ILCT electronic transitions.

Figure 4 shows the absorption spectra of compound **3** (10 μM in CH_3CN) by adding a 1:1 ratio of Li^+, Na^+, K^+, Cs^+, Mg^{2+}, Ca^{2+}, Ba^{2+}, Hg^{2+}, Pb^{2+}, Mn^{2+}, Cd^{2+}, Ag^+, Ni^{2+}, Cu^{2+}, Zn^{2+}, Co^{2+}, Cr^{3+}, Fe^{2+}, and Fe^{3+}. Among all the metal ions, Fe^{3+} affects the spectrum the most dramatically. The band at 292 nm was increased by $\sim$32% with the addition of one equivalent of Fe^{3+}. This absorption band was not specific to the Fe^{3+} and was also affected by other metal ions. On the other hand, the band at 380 nm was decreased by $\sim$25% with the addition of one equivalent Fe^{3+}, which was nonsensitive to other surveyed metal ions (around 0%–10%).

For the binding mechanism of compound **3** toward Fe^{3+}, spectrometric titration experiments were performed in the presence of Fe^{3+}. After the sequential addition of Fe^{3+} ions ranging from 0 to 3.0 equivalents, compound **3** showed a gradual increase in the absorbance of the 292 nm band and a decrease in the absorbance of 380 nm. Moreover, a new absorption peak appeared at 274 nm (Figure 5). Its intensity was increased when the sequential addition of Fe^{3+} reached 3.0 equivalents.

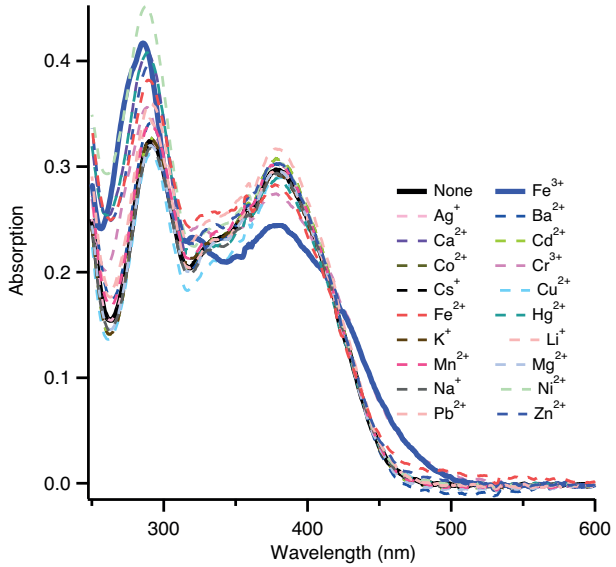

Figure 4. UV-Vis absorption change profiles of compound 3 (10.0 μM) in CH_3CN with various metal ions (10.0 μM).

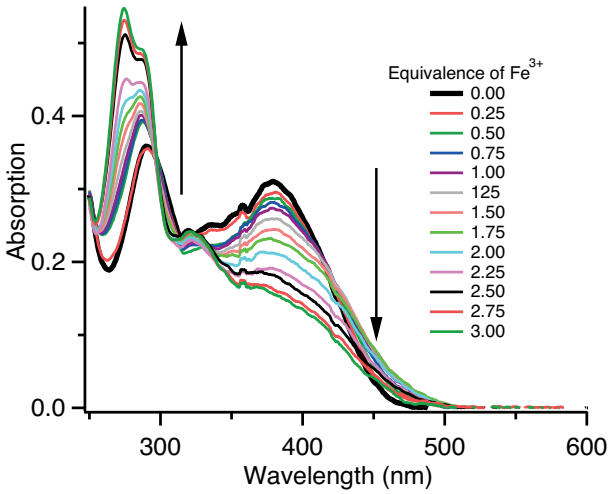

Figure 5. UV-Vis absorption spectrum of compound 3 (10.0 μM) with gradual addition of Fe^{3+} in CH_3CN solution; inset: changes of absorbance upon addition of Fe^{3+} at 380 nm.

2.3. Fluorescence properties

The emission spectrum of compound **3** showed a very weak band at 426 nm when excited at 290 nm (the solid black line in Figure 6). This weak fluorescence is due to the C=N isomerization process. Wu and coworkers sophisticatedly designed guest species that are bridged covalently and noncovalently to the C=N bond, which prevented isomerization. This eventually resulted in a dramatic increase in fluorescence. This probably occurred due to the fact that C=N isomerization was the predominant decay process of the excited states of compound **3** with an unbridged C=N structure.[37] Absorption and fluorescence bands along with Stoke's shifts are listed in Table 2. Unfortunately, the excitation at 380 nm did not give any emission. This might be due to the fact that the fluorescence band is so broad that it overlaps with the absorption band at 380 nm. This was further evaluated by measuring the fluorescence at different wavelengths that are below 380 nm so that the overlap is less.

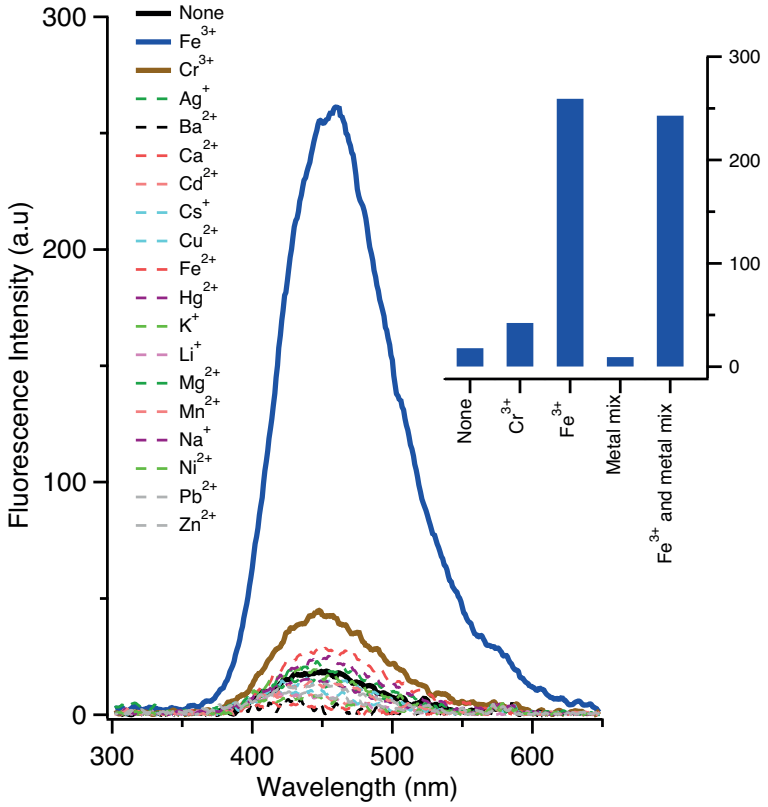

Figure 6. Fluorescence responses of compound 3 (10.0 μM) in CH_3CN solution upon the addition of 2 equiv various metal ions (excitation wavelength = 290 nm).

Each of the following cations (Li^+, Na^+, K^+, Cs^+, Mg^{2+}, Ca^{2+}, Ba^{2+}, Hg^{2+}, Pb^{2+}, Mn^{2+}, Cd^{2+}, Ag^+, Ni^{2+}, Cu^{2+}, Zn^{2+}, Co^{2+}, Cr^{3+}, Fe^{2+}, and Fe^{3+}) were tested for their fluorescence turn-on properties with compound **3** (Figure 6). In the case of Fe^{3+}, a remarkable enhancement in fluorescent intensity was observed. The quantum yield was increased up to 20-fold. This suggests that Fe^{3+} ion addition removed the inhibition of the C=N isomerization on the turned-off compound **3**. This was most likely due to the binding of Fe^{3+} in the C=N region. Compound **3** was insensitive to all other metal ions. However, we should note that the fluorescence enhancement by the Cr^{3+} ion was also not negligible (about 3-fold).

Table 2. Comparison between experimental and calculated absorption (Abs) energies, emission (Flu) energies, and Stokes shifts (SS) of compound 3 and 3+Fe^{3+} complex. All values are in electron volts.

Method		Abs.	Flu.	SS
Experiment	Compound **3**	3.26	2.86	0.41
	[**3**+Fe^{3+}]	3.26	2.79	0.48
TDDFT, vacuo	Compound **3**	3.25	2.58	0.66
TDDFT, PCM	Compound **3**	2.92	2.28	0.63

It is well defined that the interaction between transition metal ions and Schiff bases with the chelating groups is much stronger than that of other metal ions.[50] This is mostly because of the size and electronic structure of the metal ion. On the other hand, the C=N isomerization is not the ultimate mechanism that is responsible for the fluorescence turn-on and off. Most of the transition metal ions, with their open shell 3D configurations, are known as good quenchers due to the electron/energy transfer between the metal ion and the fluorophore. Therefore, this quenching mechanism might also be involved and in competition with the enhancement by C=N isomerization.[37] This might help explain the nature of different fluorescence behavior for the ferric iron among all the transition metal ions.[51]

Figure 7 shows the fluorescence titration and trend of compound **3** in ACN (10 μM) by addition of Fe^{3+} at increasing concentrations when excited at 290 nm. While the weak fluorescence band of compound **3** at 426 nm slightly red-shifts to 443 nm, the intensity increases substantially by addition of 3 equivalents of Fe^{3+}. Job's plot analyses were used to determine the binding stoichiometry between compound **3** and Fe^{3+} (inset of Figure 7). The maximum fluorescence was observed when the molar fraction of Fe^{3+} reached 0.49, which is indicative of a 1:1 stoichiometry complexation between **3** and Fe^{3+}. This stoichiometric ratio was also validated by UV-Vis absorption titration at 380 nm.

The fluorescence titration spectra can also be used to assign the association constant, K_a, for the formation of [Compound **3** - Fe^{3+}] complex using the Benesi–Hildebrand equation,[52] which is given for 1:1 association by

$$\frac{1}{I - I_0} = \frac{1}{I_{\max} - I_0} + \frac{1}{(I_{\max} - I_0)K_\alpha[Fe^{3=}]}$$

where I_0, I_{max}, and I represent fluorescence emission intensities of free compound **3**, the maximum emission intensity observed in the presence of metal ion at 443 nm (λ_{ext} = 290 nm), and apparent emission intensity at each addition of the metal ion, respectively. The binding constant was determined to be (1.36 $\pm$ 0.09).10^4 M^{-1} as shown in Figure 8a.

In order to understand the sensitivity, the fluorescence response of compound **3** upon addition of Fe^{3+} was further tested. The fluorescence intensity is proportional to the complex concentration, which linearly increases with Fe^{3+} addition (Figure 8b). In the plot, we excluded the first three points on which there were almost no fluorescence responses. The detection can readily be calculated using the formula $3\sigma/b$, where σ is the standard deviation of the blank measurements in the absence of metal ion and b is the slope in the linear graph.53 However, the calculated detection limit of 1.53 μM using such a relation may not be accurate since we did not observe significant fluorescence response up to the 6 μM of Fe^{3+} addition.

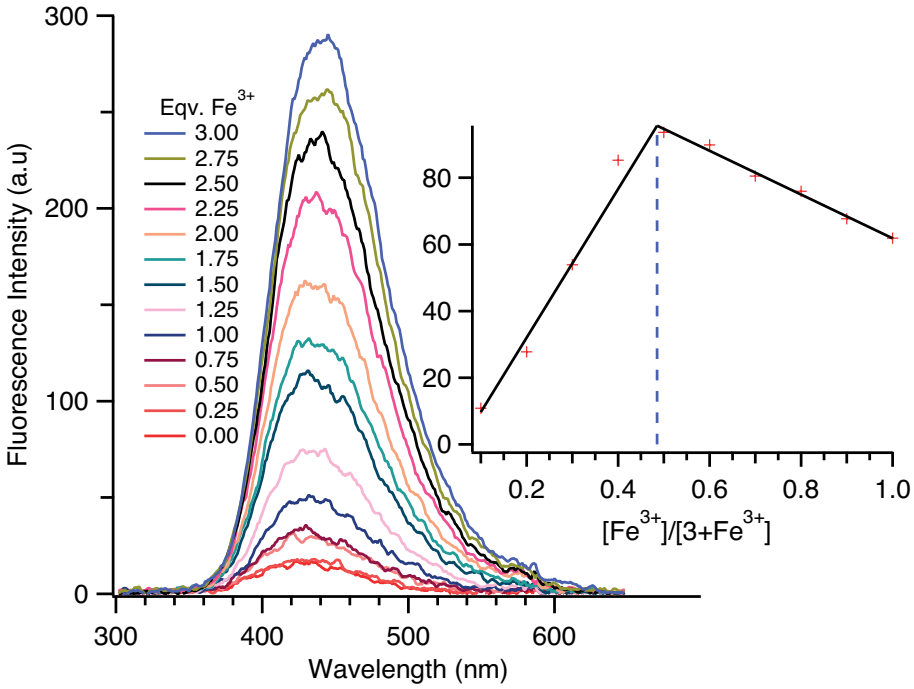

Figure 7. Fluorescence titration of compound 3 (10 μM) with various concentration of Fe^{3+} in CH_3CN solution (excitation wavelength = 290 nm).

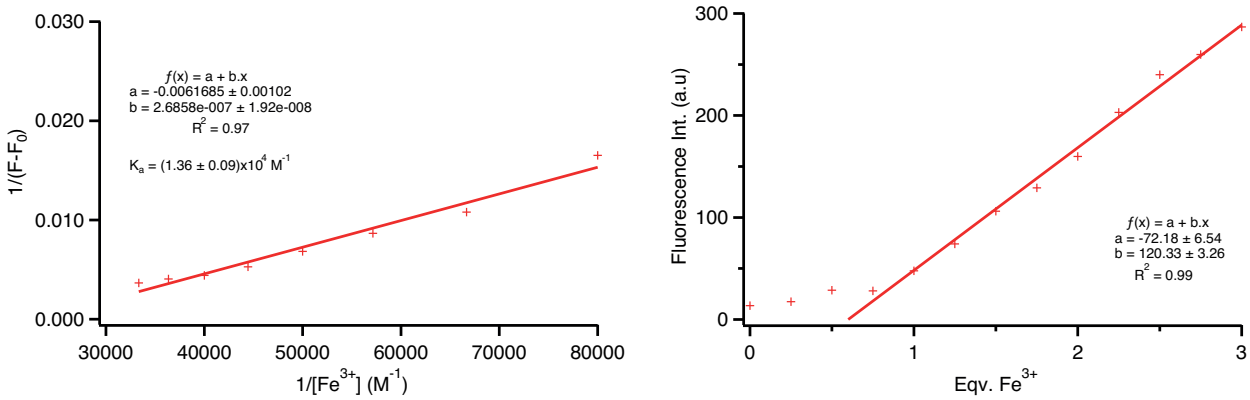

Figure 8. Plot of $1/F - F_0$ against $1/[Fe^{+3}]$ for compound 3 in CH_3CN solution.

The IR spectrum of compound **3** exhibited two characteristic bands in the region of 3360 and 3400 cm^{-1} corresponding to $-NH_2$ stretching frequencies (Figure 9). Although the crowded lower energy bands below 1700 cm^{-1} prohibit clear identification, we assigned the peak at 1679 cm^{-1} (weak–medium intense) to C=N stretching frequency with the help of DFT anharmonic frequency calculations. The following peak at 1591 cm^{-1} with a shoulder at 1619 cm^{-1} (medium intense) is likely due to $-NH_2$ bending. Upon addition of Fe^{3+}, the IR spectrum of compound **3** was perturbed. Disappearance of the peak at 3475 cm^{-1} was a clear indication that the primary amine loses one of its hydrogens. This suggests a coordination bond formation between Fe^{3+} and $-NH_2$ group (by removing a proton). Similarly, the shoulder at 1619 cm^{-1} also disappeared. Furthermore, the

C=N peak at 1679 cm^{-1} was red shifted by 42 cm^{-1}, which is indicative of a weakening C=N bond. This also suggests that Fe^{3+} is interacting with the C=N group.

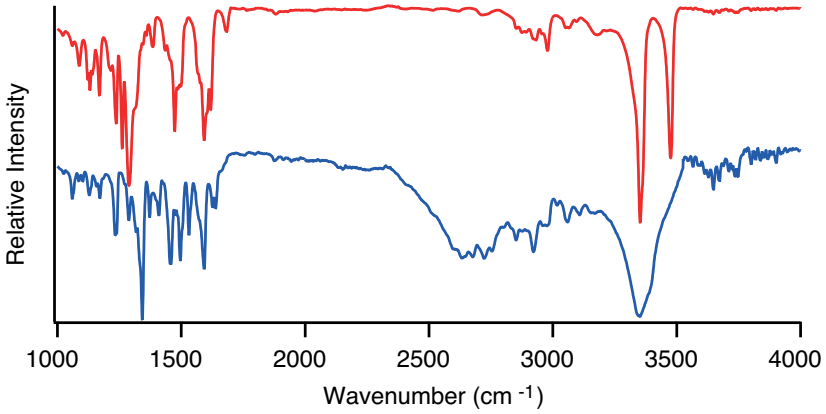

Figure 9. The IR spectrum of compound **3** and upon titration with solution Fe^{3+} ions in CH_3CN.

2.4. Binding mode

For the optimization studies, we used the B3LYP method with the basis set of LANL2TZ(f) on Fe and 6-311++G(d,p) for the rest of the atoms. Due to the limited amount of experimental information available for the compound **3+Fe**$^{3+}$ complex, the exact coordination complex structure is difficult to identify. Since there are possible square planar, tetrahedral, octahedral, and even square based pyramidal structures of transition metal ions with solvent and/or inorganic anions in the media, Fe^{3+} can complete the first coordination shell with H_2O or Cl^-. Thus, the binding of compound **3** to Fe^{3+} will be affected by these ligands. On the other hand, assuming these ligands are weaker than compound **3**, the interaction between compound **3** and Fe^{3+} will still be strong. Since our aim is limited to understanding of the qualitative interaction between the metal ion and ligand, we do not intend to identify the true coordination complex formed. To evaluate this, we compared quantum mechanical calculations on both compound **3** + Fe^{3+} and a possible tetrahedral complex formed by Cl^- ions. The optimized structures of the possible compound **3+Fe**$^{3+}$ complex are shown in Figure 10. Both in gas phase and in ACN, the geometries were optimized to their minima. In the gas phase, the distance of the Fe^{3+} to the N atom of the C=N group is 2.04 Å and to the N atom of the amine group is 1.97 Å. These values in ACN are 2.16 Å and 2.00 Å, respectively. The same distances in the Cl^- containing tetrahedral complex are 2.13 Å and 1.96 Å. Although it was irrationally high in magnitude, the calculations predicted the binding qualitatively correctly. One should also note that the Fe^{3+} has sextet state in isolated form,[54] but our calculations predict the quartet state to be more stable for Cl^--free complex whereas sextet state is more stable for the Cl^--containing complex. This spin change of iron is well known behavior and it complicates the calculations even more.[55,56]

In conclusion, a carbazole-based Schiff base with a bridged C=N structure was synthesized and characterized for recognition of Fe^{3+}. It was found that compound **3** showed a remarkable selective and sensitive response towards Fe^{3+} by using UV-vis and fluorescence methods. According to Job's plot, binding stoichiometry was 1:1. The detection limit of compound **3** was calculated as 1.0 to 6.0 μM for Fe^{3+}. The experimental observations were confirmed by density functional theory (DFT) and time-dependent density functional theory (TDDFT) calculations.

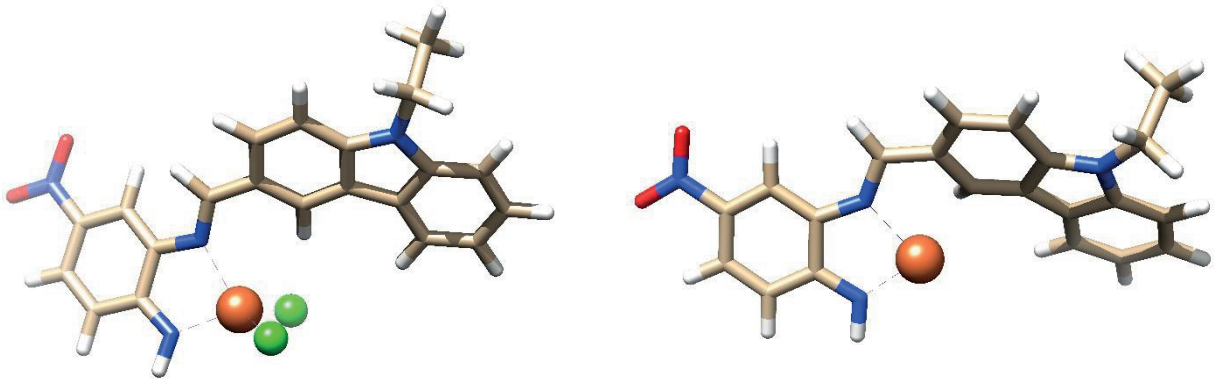

Figure 10. Optimized structure of the proposed compound $\mathbf{3} + \mathbf{Fe}^{3+}$ tetrahedral complex with 2 Cl ions.

3. Experimental and computational methods

3.1. Materials

The deuterated solvent (DMSO) for NMR spectroscopy, silica gel. and dichloromethane were provided by Merck. The following chemicals were obtained from Sigma Aldrich: 9-ethylcarbazole and 4-nitro-o-phenyldiamine. 1,8,9-Anthracenetriol for the MALDI matrix was obtained from Fluka.

Electronic absorption spectra were recorded with a Shimadzu 2101 UV spectrophotometer in the UV-visible region. Fluorescence excitation and emission spectra were recorded on a Varian Eclipse spectrofluorometer using 1-cm path length cuvettes at room temperature. Mass spectra were acquired in linear modes with average of 50 shots on a Bruker Daltonics Microflex mass spectrometer (Bremen, Germany) equipped with a nitrogen UV laser operating at 337 nm. Many different MALDI matrices were tried to find an intense molecular ion peak and low fragmentation under the MALDI-MS conditions for these compounds. ^{1}H and ^{13}C NMR spectra were recorded in DMSO solutions on a Varian 500 MHz spectrometer.

Analytical thin layer chromatography (TLC) was performed on silica gel plates (Merck, Kieselgel 60, 0.25 mm thickness) with F254 indicator. Suction column chromatography was performed on silica gel (Merck, Kieselgel 60 Å, 230–400 mesh). IR spectra were recorded on a PerkinElmer Spectrum 100 spectrophotometer.

3.2. Synthesis and characterization

The synthesis procedure for compound **2** was as follows based on the literature with a minor revision (Scheme) [42]

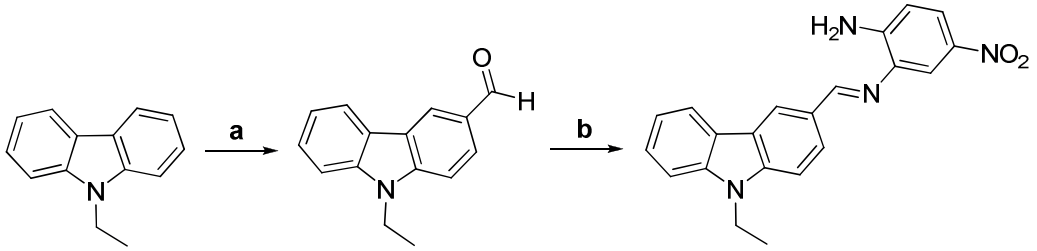

1 2 3

Scheme. Reagents and conditions: a) DMF, $POCl_3$, 100 °C, 24 h; b) DMF, nitro-o-phenyldiamine, 80 °C, 3 h.

Compound 3: A mixture of compound **2** (0.40 g., 1.79 mmol) and 4-nitro-o-phenyldiamine (0.27 g., 1.79 mmol) was heated at 80 °C in DMF (4 mL) for 3 h. The reaction mixture was poured into ice-water and

the resulting precipitate was filtered, washed with water, and dried. The crude product was purified by flash column chromatography using dichloromethane as eluent to afford the title compound as a yellow crystal. The yield was 46%. (0.29 g) IR (KBr): v_{max} 3475, 3352, 2978, 1679, 1592, 1473, 1380, 1288, 1261, 1237, 1169, 1131, 1085, 803, 746 cm^{-1}; ^{1}H NMR (500 MHz, DMSO): δ 1.33 (t, 3H, CH_3), 4.49 (q, 2H, CH_2), 6.78 (t, 2H, NH_2), 7.27 (t, H, aryl H), 7.50 (t, H, aryl H), 7.65 (d, H, J = 8.18 Hz, aryl H), 7.70 (d, H, J = 8.53 Hz, aryl H), 7.93 (d, H, J = 6.50 Hz, aryl H), 8.04 (d, H, J = 1.96 Hz, aryl H), 8.21 (t, 2H, aryl H), 8.88 (s, H, CH), 8.93 (s, H, aryl H); ^{13}C NMR (DMSO): δ 14.2 (CH_3), 37.7 (CH_2), 109.7, 110.0, 112.9, 113.0, 120.0, 121.0, 122.8, 122.9, 124.2, 126.7, 127.6, 135.1, 136.5, 140.6, 142.1, 151.4, 160.6 (aryl C and CH); Maldi (TOF); m/z 359 $[M]^+$.

3.3. X-ray data collection and structure refinement

Unit cell measurements and intensity data collection were performed on an Bruker APEX II QUAZAR three-circle diffractometer using monochromatized Mo $K\alpha$ X-radiation (λ = 0.71073 Å). Indexing was performed using APEX2.[57] Data integration and reduction were carried out with SAINT V8.34A.[58] Absorption correction was performed by multiscan method implemented in SADABS V2014/5.[59] The structures were solved and refined using the Bruker SHELXTL software package.[60] All nonhydrogen atoms were refined anisotropically using all reflections with $I > 2\sigma(I)$. The C-bound H atoms were positioned geometrically and refined using a riding mode. The N-bound H atoms were located from the difference Fourier map and restrained to be 0.89 Å from the N atom using DFIX and their position were constrained to refine on their parent N atoms with Uiso(H) = 1.2Ueq(N). Crystallographic data and refinement details of the data collection are given in Table 3. The hydrogen bonding interactions for the two compounds are shown in Table 4. The final geometrical calculations and the molecular drawings were carried out with Platon (version 1.17) and Mercury CSD (version 3.5.1).[61,62]

3.4. Absorption and emission studies

For the absorption and fluorescence studies, 278 μM stock solution of compound **3** (in acetonitrile, analytical grade, Sigma-Aldrich) was used at ambient temperature on the day of preparation. Throughout the experiments, the compound **3** concentration was constant at 10 μM and 3 repetitive measurements were made after 10 min of standard waiting time. Industrial grade metal chlorides (in water) were used in the absorption (10 μM) and fluorescence (20 μM) spectra of compound **3** in the presence of metal ions except for Ag^+ and Pb^{2+}, where nitrate salts were used. During the titration experiments with Fe^{3+} (in both absorption and fluorescence), keeping the compound **3** concentration at 10 μM, Fe^{3+} concentration was gradually increased from 0 to 30 μM (3 eq.) by 2.5 μM (0.25 eq.) additions.

3.5. Theoretical calculations

All the DFT calculations were performed by Gaussian09 v.D01 program package.[63] The geometry of compound **3** was optimized at the B3LYP hybrid functional (B3LYP) using 6-31G(d) and 6-311++G(d,p) basis sets. For **3+Fe**$^{3+}$, we used either LANL2TZ(f) triple zeta (with effective core potential (ECP) and additional f polarization functions) or LANL2DZ double zeta (with ECP) basis sets for the Fe^{3+}.[64–66] The EMSL Basis Set Library was used to retrieve the basis set data.[67,68] During the calculations, no restrictions were applied.

Table 3. Crystal data and refinement parameters for compound 3.

Empirical formula	$C_{21}H_{18}N_4O_2$
Formula weight (g.mol^{-1})	358.39
Temperature (K)	300(2)
Wavelength (Å)	0.71073
Crystal system	Monoclinic
Space group	$P\ 2_1/c$
a (Å)	15.9369(14)
b (Å)	13.4112(12)
c (Å)	16.8241(16)
α(°)	90
β(°)	100.292(6)
γ(°)	90
Crystal size (mm)	0.142 × 0.340 × 0.465
V (Å3)	3538.0(6)
Z	8
ρcalcd (g.cm^{-3})	1.346
μ (mm^{-1})	0.090
F(000)	1504
θ range for data collection (°)	2.98–25.25
h/k/l	–19/17, –16/14, –19/20
Reflections collected	22,449
Independent reflections	6362 [R(int) = 0.0622]
Absorption correction	Multiscan
Data/restraints/parameters	3132/1/204
Goodness-of-fit on F^2	1.019
Final R indices [I > 2σ(I)]	$R_1 = 0.0653$, $wR_2 = 0.1636$
R indices (all data)	$R_1 = 0.1181$, $wR_2 = 0.1966$
Largest diff. peak and hole (e.Å^{-3})	0.435 and –0.197

Table 4. Hydrogen bond parameters (Å and °) for compound 3.

D*-H$\cdots$*A	***D*-H**	**H$\cdots$*A***	***D* $\cdots$ *A***	***D*-H$\cdots$*A***
C39-H39$\cdots$O3	0.93	2.46	3.273(4)	146.0
C42-H42A$\cdots$N2	0.96	2.68	3.605(5)	161.1
N7-H1N$\cdots$O1	0.893(19)	2.16(2)	3.025(4)	163.(4)
N3-H4N$\cdots$O3	0.893(19)	2.29(3)	3.119(5)	154.(4)

In addition, symmetry constraints were removed from the calculations. Optimized structures were confirmed for their minima by harmonic frequency calculations.

In addition to the gas phase calculations, the integral equation formalism of a polarizable continuum model (IEF-PCM) was also used to include the solvent effects. The acetonitrile (ACN) parameters as implemented in Gaussian09 were used as the PCM solvent.

TDDFT calculations were performed in vacuo and solvent (ACN) environment in order to obtain the theoretical electronic absorption spectrum of compound **3**. In addition, the first low lying excited state was optimized to better understand the fluorescent behavior.

The molar extinction coefficients were calculated with the equation below, which is built in GaussView 5 software.[69] The PCM description of acetonitrile environment seems to be over-perturbing the spectrum and miscalculating the relative intensities.

$$\varepsilon_i(\tilde{\nu}) = \sum_{i=1}^{n} \left(1.3062974.10^8 \cdot \frac{f_i}{\sigma} \cdot e^{\frac{-(\tilde{\nu}-\tilde{\nu}_i)^2}{\sigma^2}} \right)$$

In the equation, σ is standard deviation (in wavenumber unit), f_i is the oscillator strength of the ith state, $\tilde{\nu}$ is the excitation energy to the ith state (in wavenumbers), and n is the number of the excited states.[70]

4. Acknowledgments

We thank the Research Fund of TÜBİTAK for the financial support given to the research project (project number: 113Z159) and allowing us to use their computer clusters and software packages for calculations. AK gratefully acknowledges Ricardo B Metz from the University of Massachusetts, for allowing him to use their computer clusters and software packages for calculations.

References

1. Gou, C.; Qin, S. H.; Wu, H. Q.; Wang, Y.; Luo, J.; Liu, X. Y. *Inorg. Chem. Comm.* **2011**, *14*, 1622-1625.
2. Ghosh, K.; Saha, I. *Tetrahedron Lett.* **2010**, *51*, 4995-4999.
3. Azadbakht, R.; Keypour, H. *Spectrocim. Acta A* **2012**, *85*, 293-297.
4. Wang, L.; Qin, W.; Liu, W. *Inorg. Chem. Comm.* **2010**, *13*, 1122-1125.
5. Bhalla, V.; Tejpal, R.; Kumar, M.; Puri, R. K.; Mahajan, R. K. *Tetrahedron Lett.* **2009**, *50*, 2649-2652.
6. Udhayakumari, D.; Saravanamoorthy, S.; Ashok, M.; Velmathi, S. *Tetrahedron Lett.* **2011**, *52*, 4631-4635.
7. Jiang, J.; Gou, C.; Luo, J.; Yi, C.; Liu, X. *Inorg. Chem. Comm.* **2012**, *15*, 12-15.
8. Delavaux-Nicot, B.; Maynadié, J.; Lavabre, D.; Fery-Forgues, S. *Inorg. Chem.* **2006**, *45*, 5691-5702.
9. An, J. M.; Yang, Z. Y.; Yan, M. H.; Li, T. R. *J. Lumin.* **2013**, *139*, 79-83.
10. Singh, T. S.; Paul, P. C.; Pramanik, H. A. R. *Spectrochim Acta A* **2014**, *121*, 520-526.
11. Cao, W.; Zheng, X. J.; Sun, J. P.; Wong, W. T.; Fang, D. C.; Zhang, J. X.; Jin, L. P. *Inorg. Chem.* **2014**, *53*, 3012-3021.
12. Mahato, P.; Saha, S.; Das, A. *J. Phys. Chem. C* **2012**, *116*, 17448-17457.
13. Dong, M.; Ma, T. H.; Zhang, A. J.; Dong, Y. M.; Wang, Y. W.; Peng, Y. *Dyes Pigm.* **2010**, *87*, 164-172.
14. Yao, J.; Dou, W.; Qin, W.; Liu, W. *Inorg. Chem. Comm.* **2009**, *12*, 116-118.
15. Richardson, D. R. *Cr. Rev. Oncol-Hem.* **2002**, *42*, 267-281.
16. Hentze, M. W.; Muckenthaler, M. U.; Andrews, N. C. *Cell* **2004**, *117*, 285-297.
17. Lieu, P. T.; Heiskala, M.; Peterson, P. A.; Yang, Y. *Mol. Asp. Med.* **2001**, *22*, 1-87.
18. Devaraj, S.; Tsui, Y. K.; Chiang, C. Y.; Yen, Y. P. *Spectrochim Acta A* **2012**, *96*, 594-599.
19. Perez, C. A.; Tong, Y.; Guo, M. *Curr. Bioac. Comp.* **2008**, *4*, 150-158.
20. 20. Marenco, M. J. C.; Fowley, C.; Hyland, B. W.; Hamilton, G. R. C.; Galindo-Riaño, D.; Callan, J. F. *Tetrahedron Lett.* **2012**, *53*, 670-673.
21. Yang, C. X.; Ren, H. B.; Yan, X. P. *Anal. Chem. (Washington, DC, U. S.)* **2013**, *85*, 7441-7446.

22. Brandel, J.; Humbert, N.; Elhabiri, M.; Schalk, I. J.; Mislin, G. L. A.; Albrecht-Gary, A. M. *Dalton Trans.* **2012**, *41*, 2820-2834.
23. Ma, Y.; Luo, W.; Quinn, P. J.; Liu, Z.; Hider, R. C. *J. Med. Chem.* **2004**, *47*, 6349-6362.
24. Qu, X.; Liu, Q.; Ji, X.; Chen, H.; Zhou, Z.; Shen, Z. *Chem. Commun. (Cambridge, U. K.)* **2012**, *48*, 4600-4602.
25. Yao, Q.; Sun, J.; Li, K.; Su, J.; Peskov, M. V.; Zou, X. *Dalton Trans.* **2012**, *41*, 3953-3955.
26. Wang, B.; Hai, J.; Liu, Z.; Wang, Q.; Yang, Z.; Sun, S. *Angew. Chem., Int. Ed.* **2010**, *49*, 4576-4578.
27. Bodenant, B.; Fages, F.; Delville, M. H. *J. Am. Chem. Soc.* **1998**, *120*, 7511-7519.
28. Mao, J.; Wang, L.; Dou, W.; Tang, X.; Yan, Y.; Liu, W. *Org. Lett.* **2007**, *9*, 4567-4570.
29. Chen, W. D.; Gong, W. T.; Ye, Z. Q.; Lin, Y.; Ning, G. L. *Dalton Trans.* **2013**, *42*, 10093-10096.
30. Weizman, H.; Ardon, O.; Mester, B.; Libman, J.; Dwir, O.; Hadar, Y.; Chen, Y.; Shanzer, A. *J. Am. Chem. Soc.* **1996**, *118*, 12368-12375.
31. Sahoo, S. K.; Sharma, D.; Bera, R. K.; Crisponi, G.; Callan, J. F. *Chem. Soc. Rev.* **2012**, *41*, 7195-7227.
32. Kim, H. N.; Lee, M. H.; Kim, H. J.; Kim, J. S.; Yoon, J. *Chem. Soc. Rev.* **2008**, *37*, 1465-1472.
33. Kumar, P.; Kumar, V.; Gupta, R. *RSC Advances* **2015**, *5*, 97874-97882.
34. Karthikeyan, M. S.; Prasad, D. J.; Poojary, B.; Subrahmanya Bhat, K.; Holla, B. S.; Kumari, N. S. *Bioorg. Med. Chem.* **2006**, *14*, 7482-7489.
35. Panneerselvam, P.; Nair, R. R.; Vijayalakshmi, G.; Subramanian, E. H.; Sridhar, S. K. *Eur. J. Med. Chem.* **2005**, *40*, 225-229.
36. Gupta, K. C.; Sutar, A. K. *Coordination Chemistry Reviews* **2008**, *252*, 1420-1450.
37. Wu, J. S.; Liu, W. M.; Zhuang, X. Q.; Wang, F.; Wang, P. F.; Tao, S. L.; Zhang, X. H.; Wu, S. K.; Lee, S. T. *Org. Lett.* **2007**, *9*, 33-36.
38. Zhang, F. F.; Gan, L. L.; Zhou, C. H. *Bioorg. Med. Chem. Lett.* **2010**, *20*, 1881-1884.
39. Kundu, P.; Justin Thomas, K. R.; Lin, J. T.; Tao, Y. T.; Chien, C. H. *Adv. Funct. Mater.* **2003**, *13*, 452.
40. Wakim, S.; Bouchard, J.; Simard, M.; Drolet, N.; Tao, Y.; Leclerc, M. *Chem. Mater.* **2004**, *16*, 4386-4388.
41. Yang, L.; Zhu, W.; Fang, M.; Zhang, Q.; Li, C. *Spectrochim Acta A* **2013**, *109*, 186-192.
42. Yu, L.; Li, L.; Fei, X. *J. Lumin.* **2014**, *149*, 28-34.
43. Asiri, A. M.; Khan, S. A.; Tan, K. W.; Ng, S. W. *Acta Crystallogr. E* **2010**, *66*, 2046.
44. Yeksan, N.; Uzkara, E.; Zeybek, O.; Asker, E. *Acta Crystallogr. E* **2010**, *66*, 1456.
45. Lauria, A.; Bonsignore, R.; Terenzi, A.; Spinello, A.; Giannici, F.; Longo, A.; Almerico, A. M.; Barone, G. *Dalton Trans.* **2014**, *43*, 6108-6119.
46. Silvestri, A.; Barone, G.; Ruisi, G.; Anselmo, D.; Riela, S.; Liveri, V. T. *J. Inorg. Biochem.* **2007**, *101*, 841-848.
47. Campbell, N. H.; Karim, N. H. A.; Parkinson, G. N.; Gunaratnam, M.; Petrucci, V.; Todd, A. K.; Vilar, R.; Neidle, S. *J. Med. Chem.* **2012**, *55*, 209-222.
48. Mitra, A.; Ramanujam, B.; Rao, C. P. *Tetrahedron Lett.* **2009**, *50*, 776-780.
49. Martin, R. L. *J. Chem. Phys.* **2003**, *118*, 4775-4777.
50. Kocak, A.; Yilmaz, H.; Faiz, O.; Andac, O. *Polyhedron* **2016**, *104*, 106-115.
51. Tan, S. S.; Kim, S. J.; Kool, E. T. *J. Am. Chem. Soc.* **2011**, *133*, 2664-2671.
52. Benesi, H. A.; Hildebrand, J. H. *J. Am. Chem. Soc.* **1949**, *71*, 2703-2707.
53. Parker, C. A.; Rees, W. T. *Analyst* **1960**, *85*, 587-600.
54. Sugar, J.; Corliss C. *J. Phys. Chem. Ref. Data 14, Suppl. 2,* 1985.
55. Altinay, G.; Citir, M.; Metz, R. B. *J. Phys. Chem. A* **2010**, *114*, 5104-5112.

56. Citir, M.; Altinay, G.; Austein-Miller, G.; Metz, R. B. *J. Phys. Chem. A* **2010**, *114*, 11322-11329.

57. Bruker APEX2, (version 2014.11.0), Bruker AXS Inc., Madison, WI, USA, 2014.

58. Bruker SAINT, (version V8.34A), Bruker AXS Inc., Madison, WI, USA, 2013.

59. Bruker SADABS, (version 2014/4), Bruker AXS Inc., Madison, WI, USA, 2014.

60. Bruker SHELXTL, (version 6.14) Bruker AXS Inc., Madison, WI, USA, 2010.

61. Spek, A. L. *Acta Crystallogr. D* **2009**, *65*, 148.

62. Macrae, C. F.; Bruno, I. J.; Chisholm, J. A.; Edgington, P. R.; McCabe, P.; Pidcock, E.; Rodriguez-Monge, L.; Taylor, R.; van de Streek, J.; Wood, P. A. *J. App. Crystallogr.* **2008**, *41*, 466-470.

63. Frisch, M. J.; Trucks, G. W.; Schlegel, H. B.; Scuseria, G. E.; Robb, M. A.; Cheeseman, J. R.; Scalmani, G.; Barone, V.; Mennucci, B.; Petersson, G. A.; et al. D.01 ed.; Gaussian, Inc.: Wallingford, CT, USA, 2013.

64. Becke, A. D. *J. Chem. Phys.* **1993**, *98*, 5648-5652.

65. Lee, C.; Yang, W.; Parr, R. G. *Phys. Rev. B* **1988**, *37*, 785-789.

66. Hay, P. J.; Wadt, W. R. *J. Chem. Phys.* **1985**, *82*, 270-283.

67. Schuchardt, K. L.; Didier, B. T.; Elsethagen, T.; Sun, L.; Gurumoorthi, V.; Chase, J.; Li, J.; Windus, T. L. *J. Chem. Inf. Model.* **2007**, *47*, 1045-1052.

68. Feller, D. *J. Comput. Chem.* **1996**, *17*, 1571-1586.

69. Dennington, R.; Keith, T.; Millam, J. *GaussView, Version 5*; Semichem Inc.: Shawnee Mission, KS, USA, 2009.

70. Stephens, P. J.; Harada, N. *Chirality* **2010**, *22*, 229-233.

Supplementary Materials

Supplementary data

CCDC 1408345 contains the supplementary crystallographic data for compound **3**. The data can be obtained free of charge via http://www.ccdc.cam.ac.uk/conts/retrieving.html, or from the Cambridge Crystallographic Data Centre, 12 Union Road, Cambridge CB2 1EZ, UK; fax: (+44) 1223-336-033; or email: deposit@ccdc.cam.ac.uk.

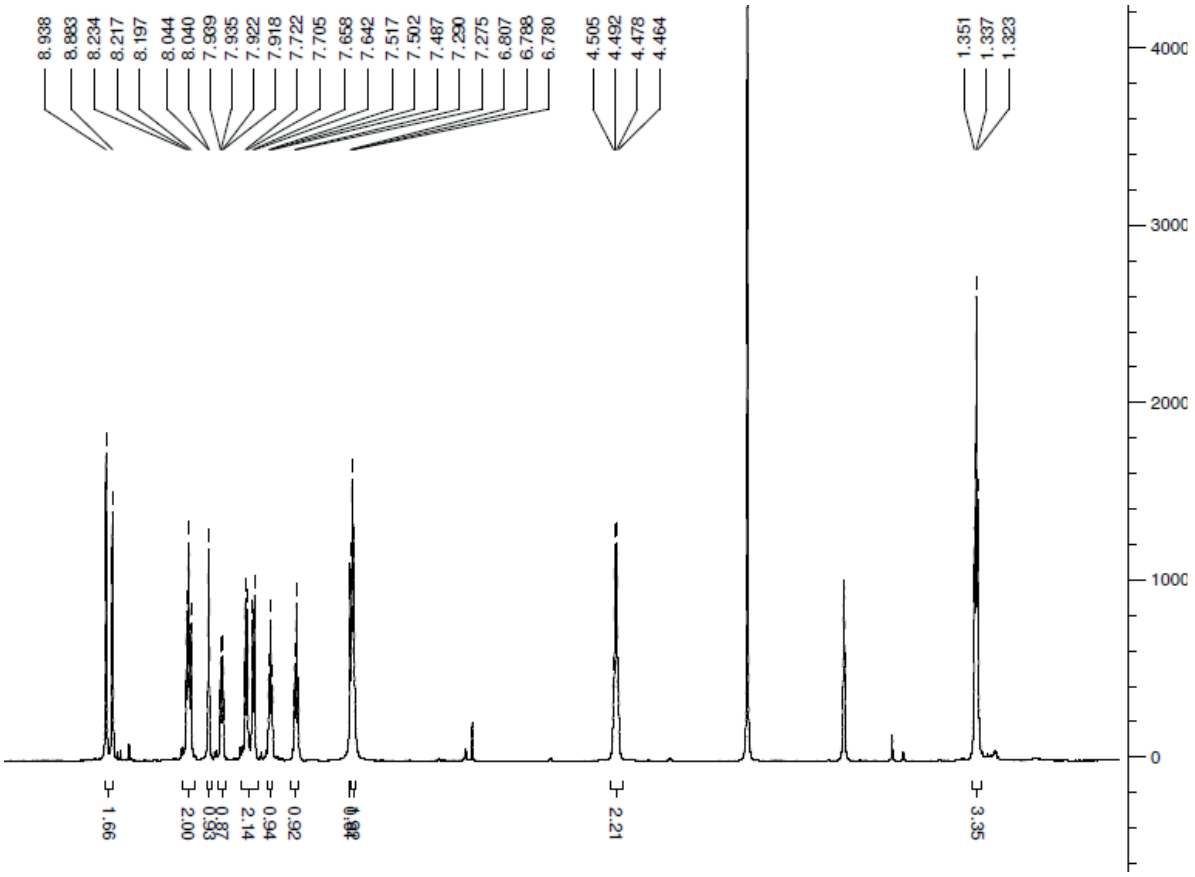

^{1}H NMR (DMSO-d$_6$) spectra of compound **3**

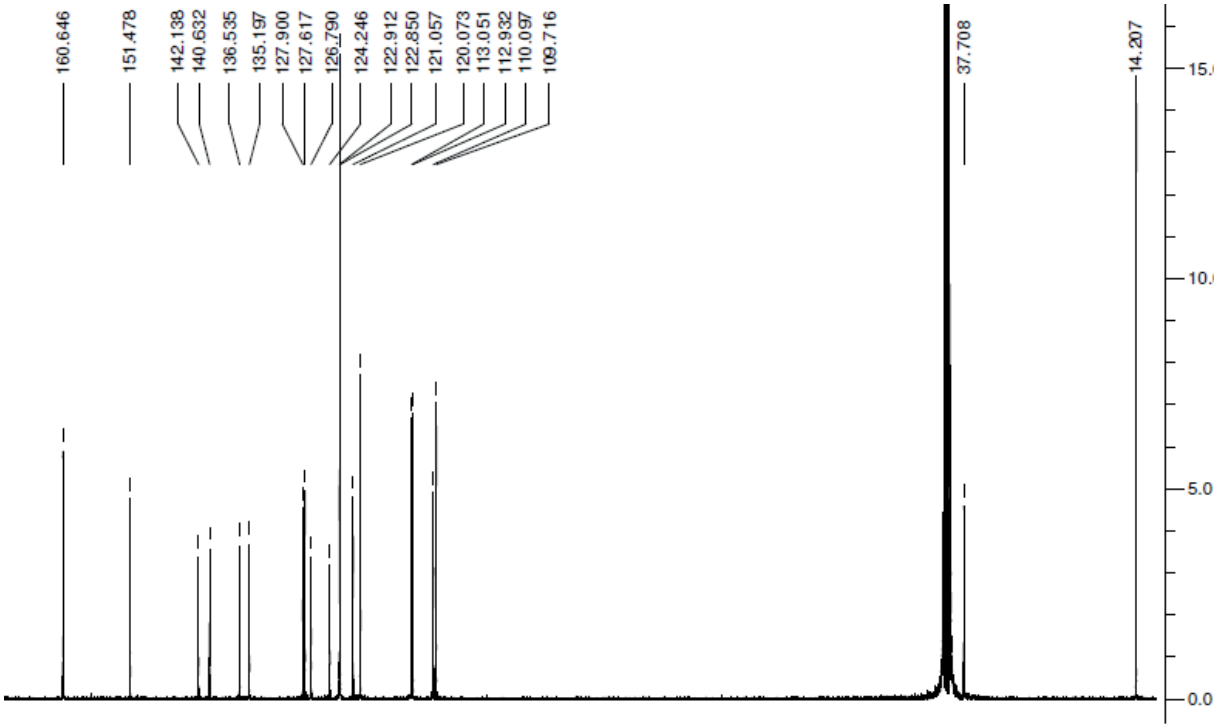

^{13}C NMR (DMSO-d_6) spectra of compound **3**

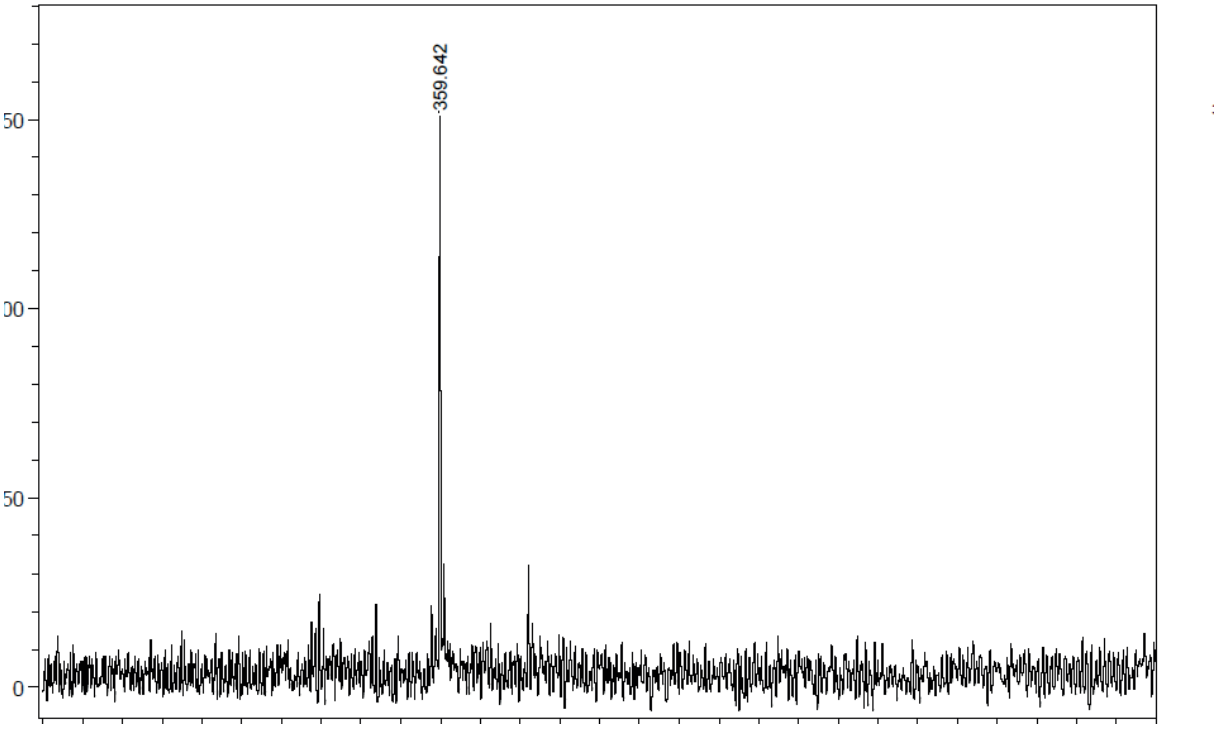

MALDI-TOF spectra of compound **3**